AGU PUBLICATIONS

Geophysical Research Letters

RESEARCH LETTER

10.1002/2016GL068786

Key Points:

- We propose a tsunami prediction approach for the near-field where current tsunami warning systems are of limited effectiveness
- The approach utilizes seismic data and minimizes assumptions on rupture dynamics, leading to rapid and robust tsunami predictions
- The approach is tested against the three tsunami events, and model predictions agree well with tsunami recordings for warning purposes

Supporting Information:

- Supporting Information S1

Correspondence to:
L. Meng,
meng@epss.ucla.edu

Citation:
An, C., and L. Meng (2016), Application of array backprojection to tsunami prediction and early warning, *Geophys. Res. Lett.*, *43*, doi:10.1002/2016GL068786.

Received 21 MAR 2016
Accepted 31 MAR 2016
Accepted article online 4 APR 2016

Application of array backprojection to tsunami prediction and early warning

Chao An[1] and Lingsen Meng[1]

[1]Earth, Planetary, and Space Sciences, UCLA, Los Angeles, California, USA

Abstract Teleseismic and static geodetic data have weak constraints on the offshore slip while tsunami data are limited by their availability, so predictions of tsunami waves in the near-field remain challenging. In this study, we develop a near-field tsunami prediction approach based on seismic array backprojections (BP). In this approach, the rupture area is first estimated by enclosing the BP radiators. Then slip models with uniform slip are constructed based on statistical scaling relations between rupture area and seismic moment to predict the near-field tsunami waveforms. The method is applied to the 2011 Tohoku, 2014 Iquique, and 2015 Illapel tsunami events, and the model predictions are compared with tsunami recordings at 57 tidal gauges and nine DART stations. Results show that the average error of arrival time and amplitude nearshore is approximately −15 to +5 min and 0.5 m, respectively, which are sufficiently small for tsunami warning purposes.

1. Introduction

Tsunamis are deadly natural hazards due to their destructive damage to coastal regions. Frequent and large tsunami hazards in the 21st century [*Wang and Liu*, 2006; *Yeh et al.*, 2007; *Fritz et al.*, 2011; *Satake*, 2014; *Leonard and Bednarski*, 2014; *Lagos and Fritz*, 2015] motivated the effort to improve the warning systems [e.g., *Titov et al.*, 2005]. The Pacific Tsunami Warning Center utilizes point sources extracted from teleseismic measurements, *P* wave magnitude (M_{wp}) and the *W* phase centroid moment tensors to issue warnings in the first hour [*Hirshorn et al.*, 2013; *Melgar et al.*, 2016a]. At large distances (∼1000 km), the NOAA system provides warnings based on water elevation data from deep ocean pressure sensors (the DART system) and precalculated Green's functions [*Titov et al.*, 2005; *Tang et al.*, 2009; *Percival et al.*, 2011]. Theoretically, the latter approach can be implemented as soon as data are collected at DART buoys, and it can achieve good performance in real time [e.g., *Wei et al.*, 2008, 2013]. In the near field (<30–60 min after earthquake) where tsunami data are not available, it is still challenging to predict site-to-site tsunami arrival time and amplitude in real time. The *W* phase solution [*Kanamori and Rivera*, 2008], which robustly determines the earthquake moment, can be obtained theoretically in a short time frame (5–15 min) depending on data availability (regional GPS, regional seismic data and teleseismic data), although it normally takes longer in a real event [e.g., ∼30 min in the 2015 Illapel event, *Melgar et al.*, 2016b]. In the absence of the slip distribution, a widely implemented approach is to precalculate a database of synthetic tsunami scenarios and chooses one scenario according to the earthquake magnitude to guide the tsunami warning [e.g., *Tatehata*, 1997; *Hoshiba and Ozaki*, 2014; *Lauterjung et al.*, 2014; *Greenslade and Titov*, 2008; *Greenslade et al.*, 2011]. Japan Meteorological Agency (JMA) operates such a warning system [*Tatehata*, 1997] which issued fast tsunami warnings during the 2011 Tohoku event, although the earthquake magnitude was underestimated. Using teleseismic data (∼15 min after earthquake), a slip model can be obtained in real time by inverting the seismic waveforms, but such inversions suffer from nonuniqueness and impose weak constraints of the final slip distribution, leading to inaccurate predictions of tsunami waves [e.g., *Lay et al.*, 2014; *An et al.*, 2014]. The real-time application of land-based GPS and strong motion recordings has also been explored for the purpose of tsunami warning [e.g., *Melgar and Bock*, 2015]; such an approach leads to a fast estimation of the fault slip distribution (<10 min), and adoption of high-rate GPS waveforms and strong motion data increases the sensitivity offshore [*Melgar and Bock*, 2015; *Melgar et al.*, 2016b], which contributes most to the tsunami generation [e.g., *Yue et al.*, 2014]. In order to collect more tsunami measurements in the near field, Japan has deployed cabled sea bottom pressure sensors between the trench and coastline [*Sato et al.*, 2011; *Maeda et al.*, 2011], which are designed to record and provide the water elevation data in real time for tsunami warning purposes [e.g., *Tsushima et al.*, 2011]. The approach was demonstrated by the retrospective analysis of the Tohoku event [*Tsushima et al.*, 2011, 2014], although the system was not able to provide real-time data during the event due to strong motion and large tsunami waves [*Tsushima et al.*, 2011].

The backprojection (BP) technique back traces the coherent *P* waves from seismic arrays to resolve the areas of strongest high-frequency radiation [e.g., *Ishii et al.*, 2005; *Allmann and Shearer*, 2007; *Meng et al.*, 2014] and constrain the spatiotemporal properties of the rupture (dimension, direction, speed, and segmentation). It only utilizes the phase of the coherent seismic waves to resolve the rupture extent, avoiding the uncertainties in finite fault inversions of seismic waves and does not rely on the details of Green's functions, parameterizations of the rupture kinematics, or additional smoothing in finite fault inversions. The only prior information required by our approach is the earthquake epicenter location that is available in real time from current earthquake early warning systems and the fault geometry that can be extracted from the slab geometries in subduction zones (e.g., Slab 1.0 model [*Hayes et al.*, 2012]). Efforts have been made to implement the BP analysis in real time [e.g., *IRIS Data Management Center*, 2011; *Wang*, 2016], and the simulation of tsunami waves can also be conducted in real time, so the procedure of our approach can be implemented depending on the availability of seismic data (<10 min using regional seismic arrays and ~15 min using teleseismic arrays). The concept is illustrated and tested for the 2011 *M* 9.0 Tohoku, 2014 *M* 8.1 Iquique, and 2015 *M* 8.2 Illapel events.

2. Method

In this section we develop the key aspects of our site-to-site tsunami prediction approach based on seismic array backprojection. This approach consists of three basic steps: (1) automatic real-time backprojection; (2) construction of a simplified earthquake source model; and (3) simulation of tsunami waves propagation.

First, the BP approach determines the locations of strong seismic radiations by analyzing the phase of *P* wave trains with array-processing techniques. In the automatic BP analysis, we adopt the correlation stacking approach to obtain robust results. The correlation stacking approach beamforms the normalized cross-correlation coefficients of waveform pairs instead of the waveforms themselves [*Frankel*, 1991; *Fletcher et al.*, 2006], leading to less affection by scattering, multipathing, and contamination of coda waves [*Borcea et al.*, 2002]. BP analysis traditionally requires seismic arrays at teleseismic distance (30–90°) for the sake of waveform simplicity and coherency. Recently, the approach has been extended to regional arrays (~10°) [*Meng et al.*, 2012, 2014]. Since regional arrays retrieve seismic data earlier (<10 min) than teleseismic arrays (~15 min), they are preferred for the tsunami warning purposes if available in the coastal regions. The seismic waves are filtered in the frequency range of 0.25–1.0 Hz for regional and 0.5–1.0 Hz for teleseismic arrays. The frequency is chosen to ensure the coherency of seismic waveforms and the spatial resolution of the BP results. By computing the stacked correlation coefficient on running windows and locating the peak correlation, the BP analysis identifies the seismic radiators if the peak correlation exceeds a prescribed threshold (0.1 for the 2011 Tohoku and 2015 Illapel events and 0.25 for the 2014 Iquique event, refer to Text S2 in the supporting information). The influence of threshold on the estimation of rupture area is analyzed in the supporting information. The automatic BP algorithm can be triggered in a real-time fashion in practical operations by the standard earthquake early warning systems (e.g., ElarmS-2 [*Kuyuk et al.*, 2013]), which also provide the epicenter location needed for the BP analysis.

A simplified source model is then constructed based on the locations of the seismic radiators. The algorithm uses an ellipse or a polygon that encloses the seismic radiators to approximate the rupture area (algorithm provided in supporting information). The seismic moment is then estimated using the scaling relation between the rupture area and seismic moment, $S_a = 2.84 \times 10^{-11} M^{2/3}$, derived based on large (*M* 6.7 to *M* 9.2) subduction-zone earthquakes [*Murotani et al.*, 2013]. Alternatively, the moment can be provided by rapid *W* phase source solutions [*Kanamori and Rivera*, 2008] if they are available in a short time frame or by estimations from geodetic measurements without saturation of displacement during large earthquakes [*Melgar et al.*, 2015]. Then the average slip D can be evaluated using the definition of seismic moment $M = \mu S_a D$, assuming a crustal rigidity μ of 32 GPa. Finally, the average slip over the elliptical or polygonal rupture area is projected to the prescribed fault geometry—a plane with strike and dip angle taken from slab geometries (e.g., Slab1.0 [*Hayes et al.*, 2012]). The rake angle is assumed to be 90° for thrust events, which can be alternatively obtained from real-time focal mechanism solutions if available. The permanent uplift/subsidence of seabed is neglected for fast warning purposes, which could be included in future efforts for more precise calculations of the runup.

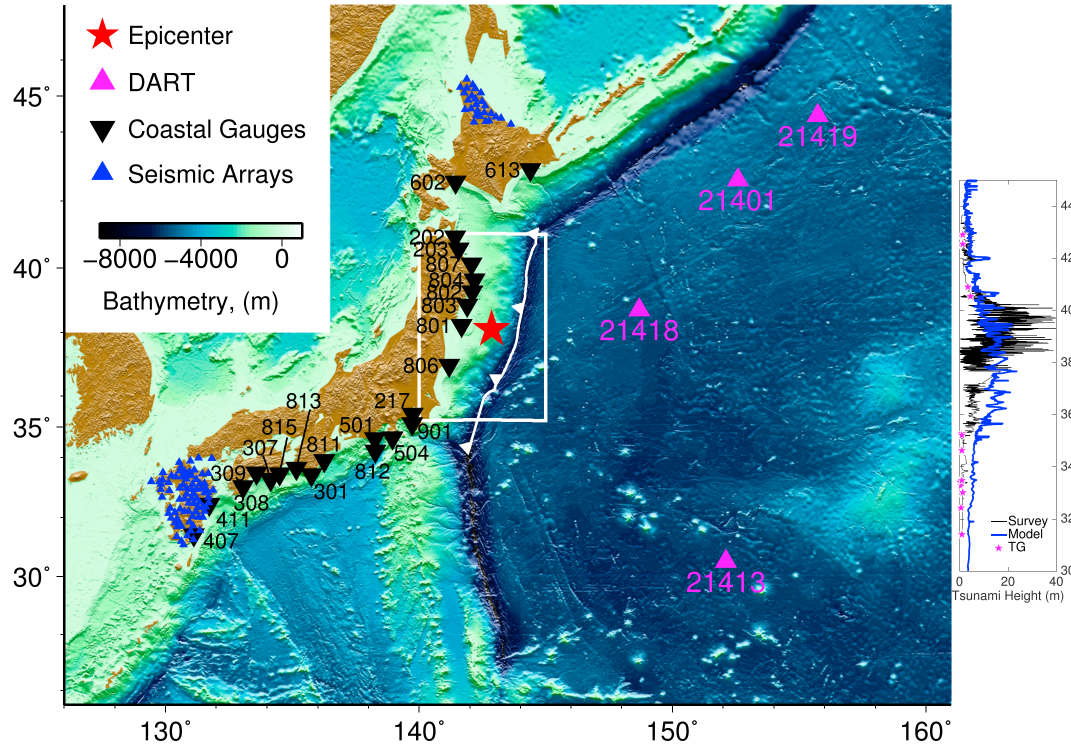

Figure 1. The seismic arrays and tsunami stations used for the 2011 Tohoku event. The red star denotes the JMA epicenter (142.86°E, 38.103°N). The blue triangles show the locations the seismic stations; the magenta triangles and black inverted triangles mark the DART stations and coastal gauges, respectively. The relevant information associated with the coastal stations (e.g., name, location, water depth, and type of sensor) can be found from http://nowphas.mlit.go.jp/chiten.htm (in Japanese). The region in the white box is displayed in Figure 2 with the earthquake source model. The right shows the runup heights computed using the ellipse source and global bathymetry with the resolution of 30 arc sec. The magenta stars in the right denote the maximum tsunami heights observed at coastal gauges.

In the third step, the generation and propagation of tsunami waves are simulated based on the input source model. We solve linear shallow water wave equations and compare the simulated and recorded tsunami waveforms at DART stations and coastal gauges. In practice, nonlinear shallow water wave equations can be solved to compute the inundation map to guide tsunami warning. We adopt the tsunami simulation package COMCOT [*Liu et al.*, 1998; *Wang and Liu*, 2006, 2007] in this approach. The bathymetry resolution is 30 arc sec extracted from the General Bathymetric Chart of the Oceans (GEBCO_08) bathymetry data; the duration of tsunami propagation is set to 14,000 s, and the time step is 0.8 s to satisfy the C.F.L. condition.

3. Case Studies

3.1. The 2011 Tohoku Earthquake

The proposed methodology is applied in a simulated real-time environment to study the 2011 *M* 9.0 Tohoku, 2014 *M* 8.1 Iquique, and 2015 *M* 8.2 Illapel events. We use two clusters of the Japanese HiNet stations to image the Tohoku earthquake, one in Kyushu and the other in northern Hokkaido, which are about 1000 km and 700 km from the epicenter, respectively (Figure 1). The tsunami recordings from 24 coastal stations and four DART stations (Figure 1) are used to compare with the model predictions.

The epicenter of (142.86°E, 38.103°N) determined by the Japan Meteorological Agency (JMA) is used. The BP analysis is first applied to the recordings of the two arrays separately and then merged to identify the locations of the seismic radiators, shown as colored circles in Figure 2a. This example was previously presented to demonstrate the regional BP imaging method using multiple arrays [*Meng et al.*, 2014]. The rupture area, defined by the ellipse or polygon that encloses the radiators, is compared with a tsunami-based slip model [*Fujii et al.*, 2011]. The ellipse and polygon agree well with the principal slip zone, although the rupture area in the south is slightly overestimated due to the southernmost backprojection radiators. The area of the ellipse

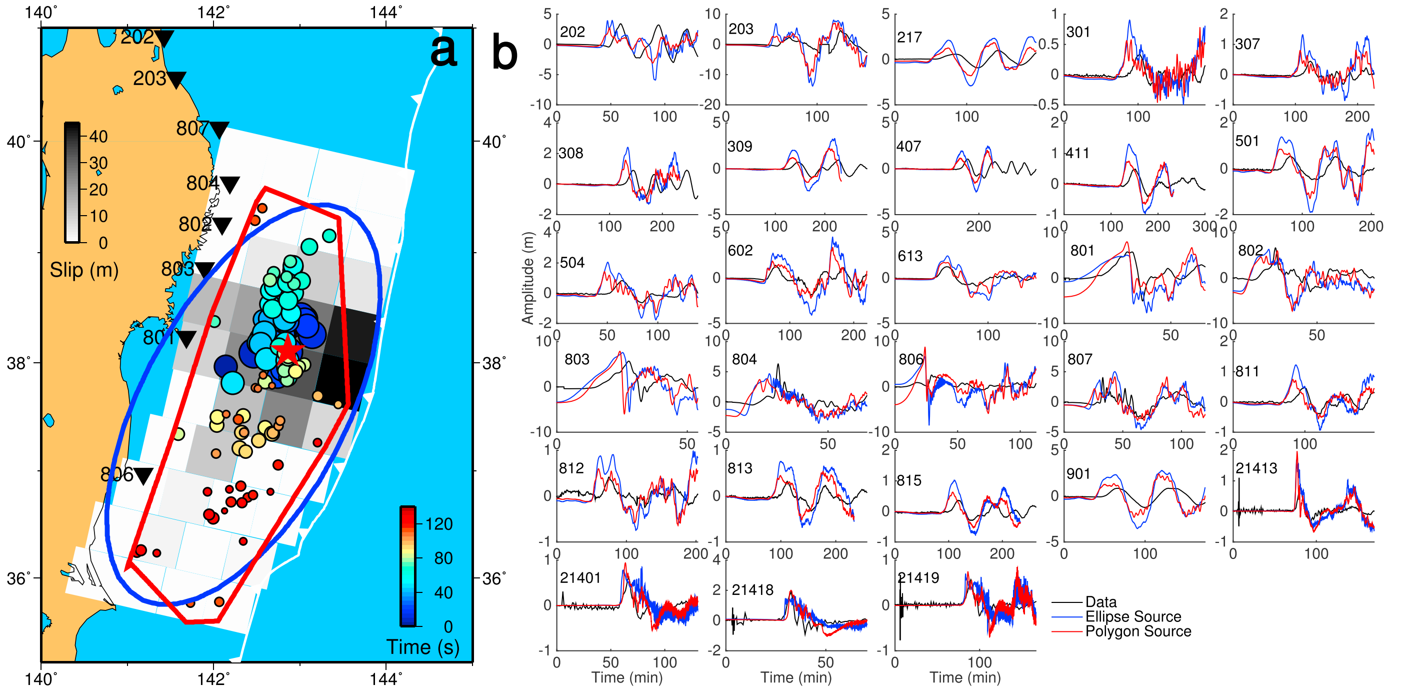

Figure 2. The earthquake source model constructed from the backprojection analysis and the prediction of tsunami waves. The colored circles mark the seismic radiators obtained from backprojection analysis, with colors denoting the rupture time. The rupture area is evaluated by the blue ellipse or the red polygon that encloses all the radiators. The slip distribution in the background is adopted from *Fujii et al.* [2011]. The records are plotted in black, and the predictions from the ellipse source and polygon source are plotted in blue and red, respectively.

and polygon is 7.64×10^4 km^2 and 5.73×10^4 km^2, respectively, corresponding to seismic moments of 6.80×10^{22} Nm (M 9.22) and 4.42×10^{22} Nm (M 9.10), average slip of 27.83 m and 24.12 m, respectively.

Using the prescribed fault surface based on the Slab 1.0 model (strike = 193°, dip = 14°) and assuming a rake angle of 90°, the two source models with uniform slip distribution are implemented in COMCOT to predict the tsunami waves, shown in Figure 2b. Both models predict similar arrival times, because the northern and southern borders of the estimated rupture zone in both models are almost the same. The rupture boundary in the north is accurately determined by the backprojection analysis, which is consistent with the tsunami-inferred source model (Figure 2a). This accuracy leads to small errors of arrival times at stations in the north (stations 602, 613 in Hokkaido). On the other hand, the southern end of the rupture area reaches beyond the Fujii model, causing earlier predictions of arrival times at stations in the south (stations 407, 411, etc., in Kyushu) and very large wave amplitude at the southern end (station 806 in Fukushima). The average error for the arrival time is 7.9 min using the ellipse source and 8.6 min using the polygon source, both of which are acceptable for early warning purposes. The average error of the tsunami amplitude is 1.2 m using the ellipse source and 0.9 m using the polygon source. The error is amplified by the less accurate predictions at several stations (e.g., 806, and 21413) due to the overestimated southern rupture zone. We also compare the runup tsunami heights along the coastline with the survey data [*Mori et al.*, 2011], shown in the right of Figure 1. The runup heights are underestimated near the source, which is largely due to the coarse bathymetry we have used (30 arc sec), because the waveforms at the coastal stations in this region (801, 802, 803, 804, and 807) have been well reproduced. The runup heights are overestimated in the south due to the same reason of overestimation of waveforms at tsunami stations in the south. Overall, considering the simplification introduced for the sake of real-time processing, we regard the predicted arrival time and amplitude as acceptable for early warning purposes.

3.2. The 2014 Iquique Earthquake

Regional seismic arrays are not available for the 2014 Iquique and 2015 Illapel events, so we use seismic data from teleseismic arrays for the backprojection analysis. The teleseismic and regional seismic arrays achieve similar quality of BP images [*Meng et al.*, 2014], although regional arrays are more preferable for tsunami warning because the travel time of regional seismic phase is significantly shorter than teleseismic waves.

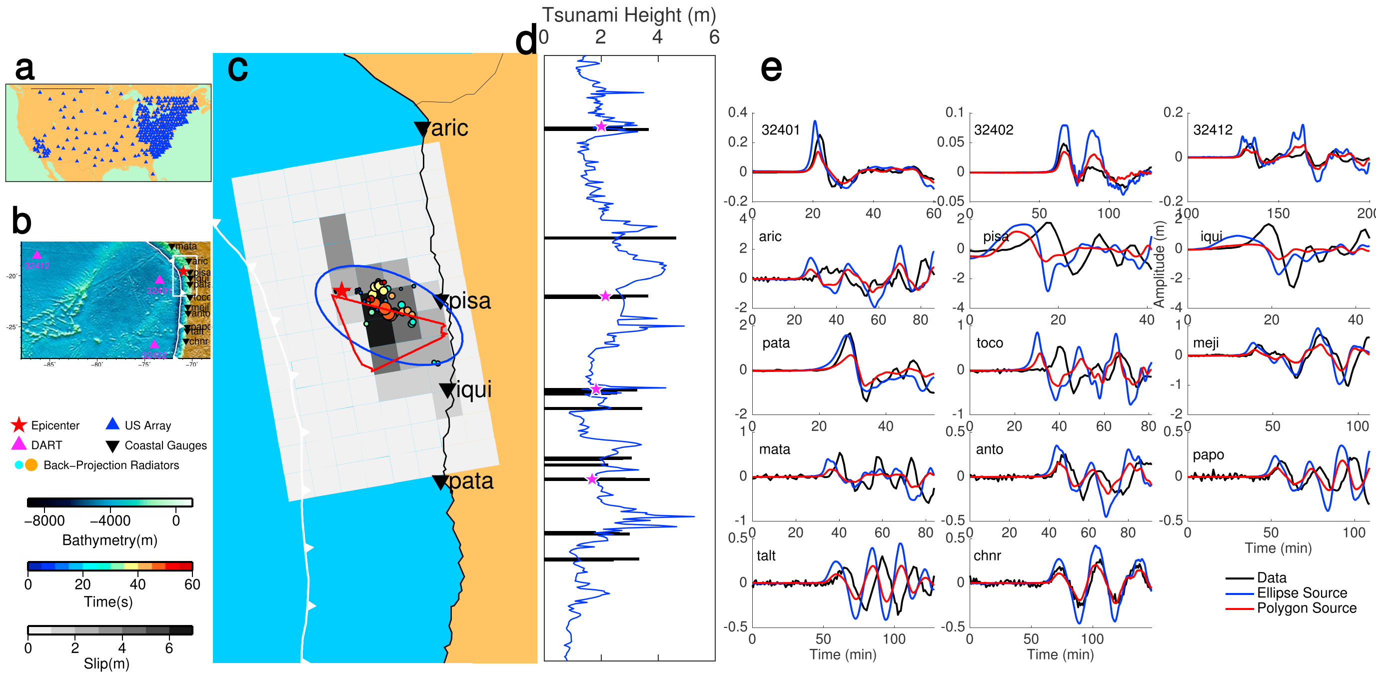

Figure 3. The seismic, tsunami stations and predicted tsunami waves for the 2014 Iquique event. (a) The USArray stations. (b) The three DART stations and 11 coastal gauges. The region in the white box is displayed in Figure 3c. (c) The backprojection analysis and estimated rupture area. The colored circles mark the seismic radiators, with colors denoting the rupture time. The rupture area is evaluated by the blue ellipse or the red polygon that encloses all the radiators. The slip distribution in the background is adopted from *An et al.* [2014]. (d) Runup heights from model predictions and surveys. The model predictions adopt the elliptical source and the global bathymetry of 30 arc sec. Magenta stars denote the maximum wave heights observed at coastal gauges. (e) Comparison of recorded and predicted tsunami waveforms. The records are plotted in black, and the predictions from the ellipse source and polygon source are plotted in blue and red, respectively.

For the 2014 Iquique event, we use the teleseismic *P* wave recordings of the USArray (Figure 3a), and the tsunami data from three DART stations and 11 coastal gauges (Figure 3b). We adopt the epicenter location determined by U.S. Geological Survey (70.817°W, 19.642°S). The seismic radiators obtained from the BP analysis are plotted in Figure 3c, along with the ellipse and polygon enclosure and the slip distribution derived from inversion of tsunami data [*An et al.*, 2014]. The ellipse covers both the region with peak slip and some areas with minor slip near the epicenter and down dip; the polygon mostly overlaps with the region of peak slip. The area of the ellipse and polygon is 5.54×10^3 km^2 and 2.71×10^3 km^2, respectively, corresponding to seismic moments of 1.33×10^{21} Nm (*M* 8.08) and 0.45×10^{21} Nm (*M* 7.77), average slip of 7.50 m and 5.24 m, respectively.

Using the prescribed fault surface from the Slab 1.0 model (strike = 350°, dip = 15°) and assuming a rake angle of 90°, the two source models with uniform slip distribution are implemented in COMCOT to predict the tsunami waves, shown in Figure 3d. Finite fault inversions reveal that the slip pattern in this event is compact near the hypocenter [*Lay et al.*, 2014; *An et al.*, 2014; *Gusman et al.*, 2015]. The rupture zone is well recovered by the BP analysis, and therefore, the arrival time is accurately predicted by both the ellipse and polygon models. The average error for the arrival time is 4.1 min using the ellipse source and 3.5 min using the polygon source. On the other hand, due to the compact slip pattern, the rupture area is slightly overestimated by the ellipse that tends to enclose more area, while underestimated by the polygon. The average amplitude error is 0.2 m using the ellipse source and 0.3 m using the polygon source. We also compare the runup tsunami heights along the coastline with the survey data [*NOAA*, 2016], shown in Figure 3d. The runup map was calculated using the global bathymetry (30 arc sec). The overall matching of predictions and runup surveys is very good. Thus, both predictions of the arrival time and wave amplitude are acceptable for warning purposes.

3.3. The 2015 Illapel Earthquake

For this event we use the USArray network (Figure 4a) and tsunami data from two DART stations and 11 coastal gauges (Figure 4b). The epicenter (71.864°W, 31.553°S) determined by the Centro Sismológico Nacional

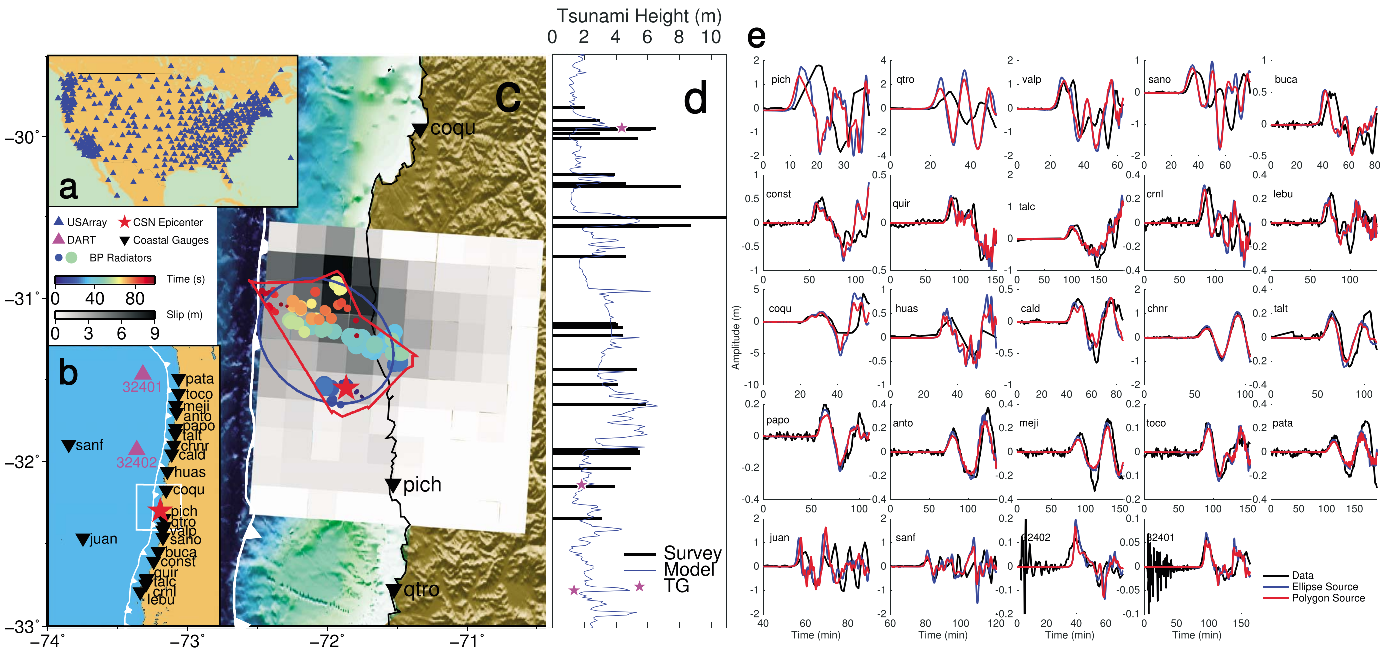

Figure 4. The seismic, tsunami stations and predicted tsunami waves for the 2015 Illapel event. (a) The USArray stations. (b) The two DART stations and 22 coastal gauges. The region in the white box is displayed in Figure 4c. (c) The backprojection analysis and estimated rupture area. The colored circles mark the seismic radiators, with colors denoting the rupture time. The rupture area is evaluated by the blue ellipse or the red polygon that encloses all the radiators. The slip distribution in the background is adopted from joint inversion of tsunami waveforms and InSAR data. (d) Runup heights from model predictions and surveys. The model predictions adopt the elliptical source and the global bathymetry of 30 arc sec. Magenta stars denote the maximum wave heights observed at coastal gauges. (e) Comparison of recorded and predicted tsunami waveforms. The records are plotted in black, and the predictions from the ellipse source and polygon source are plotted in blue and red, respectively.

is adopted. The source images obtained by the BP analysis are shown in Figure 4c. The area of the ellipse and polygon is 6.41×10^3 km^2 and 5.44×10^3 km^2, respectively, corresponding to seismic moments of 1.65×10^{21} Nm (*M* 8.15) and 1.29×10^{21} Nm (*M* 8.07), and average slip of 8.07 m and 7.43 m, respectively.

Using the prescribed fault surface from the Slab 1.0 model (strike = 4°, dip = 16°) and assuming a rake angle of 90°, the two source models with uniform slip distribution are implemented in COMCOT to predict the tsunami waves, shown in Figure 4e. The ellipse and polygon cover almost the same area that agrees well with the slip obtained from joint inversion of tsunami and InSAR data (details of the joint model are provided in the supporting information). The estimated rupture area is slightly shifted to the south, resulting in earlier predictions of arrival time at stations in the south (from "pich" to "lebu," Figure 4e). The average error of the arrival time is 1.9 min based on the ellipse source and 2.0 min using the polygon source. The average amplitude error is 0.2 m using the ellipse source and 0.1 m using the polygon source. The predictions of waveforms from the two models show excellent match with the data. We also compare the runup tsunami heights along the coastline with the survey data [*Aránguiz et al.*, 2016; *Melgar et al.*, 2016b], shown in Figure 4d. Again, the runup map was calculated using relatively coarse bathymetry (30 arc sec), so we do not expect perfect matching with the surveys. The predictions agree with the surveys very well in the south while the discrepancy is larger in the north. We observe that the peaks in the north near 30°S and 30.5°S are reproduced, albeit with smaller amplitudes.

The overall prediction errors for arrival time and amplitude of the three tsunami events are plotted in Figure 5. The arrival time can be predicted within the error of −15 to +5 min for almost all the records (Figure 5a), with only 3 exceptions out of 132 counts (2%, Figure 5c). Figure 5b shows that amplitude error is generally smaller than 0.5 m. In particular, 50 of 132 counts (38%) have almost zero amplitude error (~−0.05 m), and 81 counts (61%) have error smaller than 0.2 m, shown in Figure 5d. To summarize, our proposed array-based approach of tsunami predictions predicts reasonably accurate tsunami arrival time and amplitude. It is therefore suitable for tsunami warning purposes.

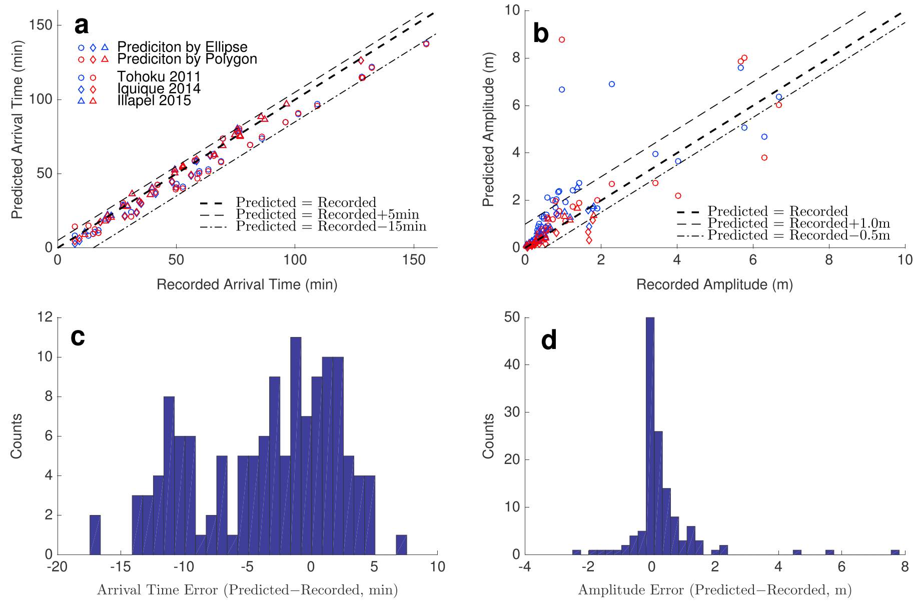

Figure 5. Prediction error for arrival time and amplitude in three tsunami events. (a) Predicted arrival time versus recorded arrival time; (b) predicted amplitude versus recorded amplitude; (c) histogram of prediction error of arrival time; and (d) histogram of prediction error of amplitude.

4. Conclusion and Discussion

In this study, we propose a site-to-site tsunami prediction approach for the purpose of near-field tsunami warning based on the backprojection analysis. In this approach, the rupture area is approximated using an ellipse or polygon to enclose all the seismic radiators obtained from the BP analysis. Then, the average slip over the rupture area is inferred based on an empirical scaling relation between the seismic moment and rupture area. Given a prescribed fault surface, which can be extracted from the slab geometries, a simple slip model with uniform slip over the rupture area is constructed to predict the tsunami waves. The approach is applied in a simulated real-time environment to the 2011 Tohoku, 2014 Iquique, and 2015 Illapel tsunami events. We find that the error of predicted arrival time is within −15 to +5 min; the amplitude is accurately predicted with errors around 0.05 m at approximately 40% of the stations; the error of the amplitude is less than 0.2 m at 60% of the stations. We consider this prediction accuracy is reasonably good for the purpose of tsunami warning. Here we also point out that all the errors mentioned in this study are calculated at coastal gauges or DART buoy stations, so the error of actual runup height could be different due to the shoaling of waves.

This array-based tsunami warning approach relies on two basic assumptions: (1) the locations of strong seismic radiation inferred BP analysis represents the rupture area; and (2) tsunami waves are not sensitive to the detailed slip distribution, and a simplified source model of uniform slip reasonably predicts the tsunami waveforms. Regarding the first assumption, it has been widely recognized that seismic data with high frequency are more efficiently generated by the abrupt change in rupture speed during the dynamic rupture rather than by total large slip [e.g., *Madariaga*, 1983]. Thus, the backprojection analysis using high-frequency seismograms is typically assumed to track the migration of the rupture front instead of recovering regions with high rupture slip. However, tracking the rupture front marks the fault extent involved in the earthquake, and therefore, the BP analysis leads to a reasonable estimation of the rupture area. Regarding the second assumption, tsunami waves are typically dominated by components of very long wavelength (>100 km), and hence, they have low spatial resolution. *An* [2015] shows that in finite fault inversions of tsunami waveforms, coarsening the subfault size from 25 km × 25 km to 100 km × 100 km in the 2011 Tohoku event and from 20 km × 20 km to 60 km × 60 km in the 2014 Iquique event hardly affects the predictions of tsunami waveforms. For the coarsest subfault grids, the final slip model has only 2–3 patches with nonzero slip. Thus, it is inferred that the tsunami waveforms can be relatively accurately simulated without the detailed knowledge of the slip distribution. This is illustrated in our case studies, where the tsunami arrival time and wave amplitude are reasonably predicted with a uniform slip model for tsunami warning purposes.

We have also evaluated the real-time capability of this approach. The first two steps, i.e., the BP analysis and the construction of source models, can be done almost instantly as long as the earthquake unfolds. The simulation of tsunami waves takes less than 2 min, and the computational time can be reduced by excluding the DART stations in practical operations. Assuming a source duration of 2 min, the collection of seismic data takes approximately 7 min using regional seismic arrays (5 min for the travel time of *Pn* wave in 10°), so the prediction of tsunami waves can be obtained approximately 9 min after earthquake occurrence; using teleseismic arrays, the collection of seismic data takes approximately 17 min, so the prediction of tsunami waves can be obtained 19 min after an earthquake. Therefore, our proposed array-based tsunami prediction approach is expected to deliver timely predictions between 9 and 19 min after an earthquake.

The array-based tsunami warning approach provides robust predictions of tsunami arrival time and amplitude in a shorter time frame (9–19 min) than current tsunami warning systems based on inversions of tsunami measurements (30–60 min). The regional BP analysis requires multiple clusters of seismometers located at regional distance from the earthquakes. Each regional array should be composed by at least a dozen of seismometers with a spacing smaller than 50 km. For the two Chilean tsunamis, such station density is only available near Santiago, which is too far to the Iquique and too close to the Illapel events. Our method can work as an important alternative tsunami warning mechanism for near-field areas where tsunami waves strike earlier than tsunami sensors in the open ocean. About 30–60 min after an earthquake, tsunami data become available and tsunami predictions can be made based on tsunami records. Our approach also provides an independent comparison, as inversions using tsunami data from only a few tsunami sensors (1–2) could be unstable.

Acknowledgments
This work made use of GMT software. The IRIS and Japanese HiNet data centers were used to access the seismic data. The tsunami data at DART stations were downloaded from NOAA's website; the tsunami data at coastal gauges in the 2011 Tohoku event were downloaded from the Nationwide Ocean Wave Information Network for Ports and Harbours, Japan (NOWPHAS); the tsunami data at coastal gauges in the 2014 Iquique and 2015 Illapel events were downloaded from the IOC's website. The simulation of tsunami waves was carried out on supercomputer Stampede. This work is supported by the Hellman fellowship and the UCLA faculty research grant. We thank Diego Melgar and an anonymous reviewers for constructive reviews.

References

Allmann, B. P., and P. M. Shearer (2007), A high-frequency secondary event during the 2004 Parkfield earthquake, *Science*, *318*(5854), 1279–1283.

An, C. (2015), Inversion of tsunami waveforms and tsunami warning, PhD thesis, Cornell University, Ithaca, N. Y.

An, C., I. Sepúlveda, and P. L.-F. Liu (2014), Tsunami source and its validation of the 2014 Iquique, Chile, earthquake, *Geophys. Res. Lett.*, *41*, 3988–3994, doi:10.1002/2014GL060567.

Aránguiz, R., et al. (2016), The 16 September 2015 Chile tsunami from the post-tsunami survey and numerical modeling perspectives, *Pure Appl. Geophys.*, *173*, 333–348.

Borcea, L., G. Papanicolaou, C. Tsogka, and J. Berryman (2002), Imaging and time reversal in random media, *Inverse Prob.*, *18*(5), 1247–1279.

Fletcher, J. B., P. Spudich, and L. M. Baker (2006), Rupture propagation of the 2004 Parkfield, California, earthquake from observations at the UPSAR, *Bull. Seismol. Soc. Am.*, *96*(4B), S129–S142.

Frankel, A. (1991), High-frequency spectral falloff of earthquakes, fractal dimension of complex rupture, b value, and the scaling of strength on faults, *J. Geophys. Res.*, *96*(B4), 6291–6302.

Fritz, H. M., et al. (2011), Field survey of the 27 February 2010 Chile tsunami, *Pure Appl. Geophys.*, *168*(11), 1989–2010.

Fujii, Y., K. Satake, S. Sakai, M. Shinohara, and T. Kanazawa (2011), Tsunami source of the 2011 off the Pacific coast of Tohoku earthquake, *Earth Planets Space*, *63*(7), 815–820.

Greenslade, D. J., and V. V. Titov (2008), A comparison study of two numerical tsunami forecasting systems, *Pure Appl. Geophys.*, *165*(11–12), 1991–2001.

Greenslade, D. J., S. C. Allen, and M. A. Simanjuntak (2011), An evaluation of tsunami forecasts from the T2 scenario database, *Pure Appl. Geophys.*, *168*(6–7), 1137–1151.

Gusman, A. R., S. Murotani, K. Satake, M. Heidarzadeh, E. Gunawan, S. Watada, and B. Schurr (2015), Fault slip distribution of the 2014 Iquique, Chile, earthquake estimated from ocean-wide tsunami waveforms and GPS data, *Geophys. Res. Lett.*, *42*, 1053–1060, doi:10.1002/2014GL062604.

Hayes, G. P., D. J. Wald, and R. L. Johnson (2012), Slab1. 0: A three-dimensional model of global subduction zone geometries, *J. Geophys. Res.*, *117*, B01302, doi:10.1029/2011JB008524.

Hirshorn, B., S. Weinstein, and S. Tsuboi (2013), On the application of Mwp in the near field and the March 11, 2011 Tohoku earthquake, *Pure Appl. Geophys.*, *170*(6–8), 975–991.

Hoshiba, M., and T. Ozaki (2014), Earthquake early warning and tsunami warning of the Japan Meteorological Agency, and their performance in the 2011 off the Pacific coast of Tohoku earthquake (Mw 9.0), in *Early Warning for Geological Disasters: Scientific Methods and Current Practice*, edited by F. Wenzel and J. Zschau, pp. 1–28, Springer, Berlin.

IRIS Data Management Center (2011), Data services products: Backprojection P-wave back-projection rupture imaging, Washington, D. C., doi:10.17611/DP/BP.1. [Available at https://ds.iris.edu/ds/products/backprojection/, accessed: 2016-03-15.]

Ishii, M., P. M. Shearer, H. Houston, and J. E. Vidale (2005), Extent, duration and speed of the 2004 Sumatra–Andaman earthquake imaged by the Hi-Net array, *Nature*, *435*(7044), 933–936.

Kanamori, H., and L. Rivera (2008), Source inversion of W phase: speeding up seismic tsunami warning, *Geophys. J. Int.*, *175*(1), 222–238.

Kuyuk, H. S., R. M. Allen, H. Brown, M. Hellweg, I. Henson, and D. Neuhauser (2013), Designing a network-based earthquake early warning algorithm for California: ElarmS-2, *Bull. Seismol. Soc. Am.*, *104*, 162–173.

Lagos, M., and H. M. Fritz (2015), One year after the 1 April 2014 Iquique tsunami field survey along the coasts of Chile and Peru, EGU General Assembly Conference Abstracts 8139, Vienna, Austria, 12–17 Apr.

Lauterjung, J., A. Rudloff, U. Münch, and D. J. Acksel (2014), The earthquake and tsunami early warning system for the Indian Ocean (GITEWS), in *Early Warning for Geological Disasters: Scientific Methods and Current Practice*, edited by F. Wenzel and J. Zschau, pp. 165–178, Springer, Berlin.

Lay, T., H. Yue, E. E. Brodsky, and C. An (2014), The 1 April 2014 Iquique, Chile, M_w 8.1 earthquake rupture sequence, *Geophys. Res. Lett.*, *41*, 3818–3825, doi:10.1002/2014GL060238.

Leonard, L., and J. Bednarski (2014), Field survey following the 28 October 2012 Haida Gwaii tsunami, *Pure Appl. Geophys.*, *171*(12), 3467–3482.

Liu, P., S. Woo, and Y. Cho (1998), *Computer Programs for Tsunami Propagation and Inundation*, Cornell University, Ithaca, N. Y.

Madariaga, R. (1983), High frequency radiation from dynamic earthquake fault models, *Ann. Geophys.*, *1*(1), 17–23.

Maeda, T., T. Furumura, S. Sakai, and M. Shinohara (2011), Significant tsunami observed at ocean-bottom pressure gauges during the 2011 off the Pacific coast of Tohoku earthquake, *Earth Planets Space*, *63*(7), 803–808.

Melgar, D., and Y. Bock (2015), Kinematic earthquake source inversion and tsunami runup prediction with regional geophysical data, *J. Geophys. Res. Solid Earth*, *120*, 3324–3349, doi:10.1002/2014JB011832.

Melgar, D., B. W. Crowell, J. Geng, R. M. Allen, Y. Bock, S. Riquelme, E. M. Hill, M. Protti, and A. Ganas (2015), Earthquake magnitude calculation without saturation from the scaling of peak ground displacement, *Geophys. Res. Lett.*, *42*, 5197–5205, doi:10.1002/2015GL064278.

Melgar, D., et al. (2016a), Local tsunami warnings: Perspectives from recent large events, *Geophys. Res. Lett.*, *43*, 1109–1117, doi:10.1002/2015GL067100.

Melgar, D., W. Fan, S. Riquelme, J. Geng, C. Liang, M. Fuentes, G. Vargas, R. M. Allen, P. M. Shearer, and E. J. Fielding (2016b), Slip segmentation and slow rupture to the trench during the 2015, M_w8.3 Illapel, Chile earthquake, *Geophys. Res. Lett.*, *43*, 961–966, doi:10.1002/2015GL067369.

Meng, L., J.-P. Ampuero, A. Sladen, and H. Rendon (2012), High-resolution backprojection at regional distance: Application to the Haiti M7.0 earthquake and comparisons with finite source studies, *J. Geophys. Res.*, *117*, B04313, doi:10.1029/2011JB008702.

Meng, L., R. Allen, and J.-P. Ampuero (2014), Application of seismic array processing to earthquake early warning, *Bull. Seismol. Soc. Am.*, *104*(5), 2553–2561.

Mori, N., T. Takahashi, T. Yasuda, and H. Yanagisawa (2011), Survey of 2011 Tohoku earthquake tsunami inundation and run-up, *Geophys. Res. Lett.*, *38*, L00G14, doi:10.1029/2011GL049210.

Murotani, S., K. Satake, and Y. Fujii (2013), Scaling relations of seismic moment, rupture area, average slip, and asperity size for $M \sim 9$ subduction-zone earthquakes, *Geophys. Res. Lett.*, *40*, 5070–5074, doi:10.1002/grl.50976.

NOAA (2016), National Geophysical Data Center/World Data Service (NGDC/WDS): Global historical tsunami database, National Geophysical Data Center, Boulder, Colo., doi:10.7289/V5PN93H7. [Available at https://www.ngdc.noaa.gov/hazard/ tsu_db.shtml, accessed: 2016-03-09.]

Percival, D. B., D. W. Denbo, M. C. Eblé, E. Gica, H. O. Mofjeld, M. C. Spillane, L. Tang, and V. V. Titov (2011), Extraction of tsunami source coefficients via inversion of DART® buoy data, *Nat. Hazards*, *58*(1), 567–590.

Satake, K. (2014), The 2011 Tohoku, Japan, earthquake and tsunami, in *Extreme Natural Hazards, Disaster Risks and Societal Implications*, vol. 1, edited by A. Ismail-Zadeh et al., pp. 310–321, Cambridge Univ. Press.

Sato, M., T. Ishikawa, N. Ujihara, S. Yoshida, M. Fujita, M. Mochizuki, and A. Asada (2011), Displacement above the hypocenter of the 2011 Tohoku-Oki earthquake, *Science*, *332*(6036), 1395–1395.

Tang, L., V. Titov, and C. Chamberlin (2009), Development, testing, and applications of site-specific tsunami inundation models for real-time forecasting, *J. Geophys. Res.*, *114*, C12025, doi:10.1029/2009JC005476.

Tatehata, H. (1997), The new tsunami warning system of the Japan Meteorological Agency, in *Perspectives on Tsunami Hazard Reduction: Observations, Theory and Planning*, edited by G. T. Hebenstreit, pp. 175–188, Springer, Netherlands.

Titov, V. V., F. I. Gonzalez, E. Bernard, M. C. Eble, H. O. Mofjeld, J. C. Newman, and A. J. Venturato (2005), Real-time tsunami forecasting: Challenges and solutions, *Natural Hazards*, *35*, 41–58.

Tsushima, H., K. Hirata, Y. Hayashi, Y. Tanioka, K. Kimura, S. Sakai, M. Shinohara, T. Kanazawa, R. Hino, and K. Maeda (2011), Near-field tsunami forecasting using offshore tsunami data from the 2011 off the Pacific coast of Tohoku earthquake, *Earth Planets Space*, *63*(7), 821–826.

Tsushima, H., R. Hino, Y. Ohta, T. Iinuma, and S. Miura (2014), tFISH/RAPiD: Rapid improvement of near-field tsunami forecasting based on offshore tsunami data by incorporating onshore GNSS data, *Geophys. Res. Lett.*, *41*, 3390–3397, doi:10.1002/2014GL059863.

Wang, D. (2016), Real time back-projection, University of Tokyo, Tokyo, Japan. [Available at http://gachon.eri.u-tokyo.ac.jp/∼dunwang, accessed: 2016-03-19.]

Wang, X., and P. L.-F. Liu (2006), An analysis of 2004 Sumatra earthquake fault plane mechanisms and Indian ocean tsunami, *J. Hydraul. Res.*, *44*(2), 147–154.

Wang, X., and P. L.-F. Liu (2007), Numerical simulations of the 2004 Indian ocean tsunamis-coastal effects, *J. Earthquake Tsunami*, *1*(3), 273–297.

Wei, Y., E. N. Bernard, L. Tang, R. Weiss, V. V. Titov, C. Moore, M. Spillane, M. Hopkins, and U. Kânoğlu (2008), Real-time experimental forecast of the Peruvian tsunami of August 2007 for U.S. coastlines, *Geophys. Res. Lett.*, *35*, L04609, doi:10.1029/2007GL032250.

Wei, Y., C. Chamberlin, V. V. Titov, L. Tang, and E. N. Bernard (2013), Modeling of the 2011 Japan tsunami: Lessons for near-field forecast, *Pure Appl. Geophys.*, *170*(6–8), 1309–1331.

Yeh, H., M. Francis, C. Peterson, T. Katada, G. Latha, R. Chadha, J. Singh, and G. Raghuraman (2007), Effects of the 2004 great Sumatra tsunami: Southeast Indian coast, *J. Waterw. Port Coastal Ocean Eng.*, *133*(6), 382–400.

Yue, H., T. Lay, L. Rivera, C. An, C. Vigny, X. Tong, and J. C. Báez Soto (2014), Localized fault slip to the trench in the 2010 Maule, Chile $M_w = 8.8$ earthquake from joint inversion of high-rate GPS, teleseismic body waves, InSAR, campaign GPS, and tsunami observations, *J. Geophys. Res. Solid Earth*, *119*, 7786–7804, doi:10.1002/2014JB011340.